Nonfullerene acceptors from thieno[3,2-b]thiophene-fused naphthalene donor core with six-member-ring connection for efficient organic solar cells

Du, Siying; Yao, Nannan; Liu, Shungang; Xu, Yongzhuo; Cao, Jiamin; Zhuang, Wenliu; Yu, Junting; Wang, Nong; Yu, Donghong; Zhang, Fengling; Wang, Ergang

Published in:
Dyes and Pigments

DOI (link to publication from Publisher):
10.1016/j.dyepig.2020.108892

Publication date:
2021

Document Version
Accepted author manuscript, peer reviewed version

Nonfullerene acceptors from thieno[3,2-*b*]thiophene-fused naphthalene donor core with six-member-ring connection for efficient organic solar cells

Siying Du[a], Nannan Yao[b], Shungang Liu[a], Yongzhuo Xu[a], Jiamin Cao[a,c]*, Wenliu Zhuang[c,d]*, Junting Yu[a], Nong Wang[c,e]*, Donghong Yu[f], Fengling Zhang[b]*, Ergang Wang[c,g]

[a] *Key Laboratory of Theoretical Organic Chemistry and Functional Molecule of Ministry of Education, School of Chemistry and Chemical Engineering, Hunan University of Science and Technology, Xiangtan 411201, China*

[b] *Department of Physics, Chemistry and Biology, Linköping University, Linköping SE-58183, Sweden*

[c] *Department of Chemistry and Chemical Engineering/Applied Chemistry, Chalmers University of Technology, Göteborg SE-41296, Sweden*

[d] *Advanced Research Center for Polymer Processing Engineering of Guangdong Province, Guangdong Industry Polytechnic, Guangzhou 510300, China*

[e] *School of Chemical and Biological Engineering, Lanzhou Jiaotong University, Lanzhou, Gansu 730070, China*

[f] *Department of Chemistry and Bioscience, Aalborg University, Aalborg East, DK-9220, Denmark*

[g] *School of Materials Science and Engineering, Zhengzhou University, Zhengzhou 450001, China*

Corresponding author:

E-mail address: minjiacao@163.com (J. Cao), w.zhuang@live.com (W. Zhuang),

wangnong07@163.com (N. Wang), fengling.zhang@liu.se (F. Zhang)

Abstract: Comprehensive design ideas on the fused-ring donor-core in state-of-the-art acceptor-donor-acceptor (A-D-A) nonfullerene acceptors (NFAs) are still of great importance for regulating the electron push-pull effect for the sake of optimal light-harvesting, frontier molecular orbital levels, and finally their photovoltaic properties. Herein, thieno[3,2-*b*]thiophenes were fused in bay-area of naphthalene *via* six-member-ring connection, resulting the formation of dihydropyrenobisthieno[3,2-*b*]thiophene based octacyclic ladder-type donor core, which was flanked by two 1,1-dicyanomethylene-3-indanone (IC) acceptor motifs with and without 5,6-diflourination, namely **PTT-IC** and **PTT-2FIC**, respectively, as novel efficient A-D-A fused-ring electron acceptors (FREAs). Compared with **PTT-IC**, fluorinated **PTT-2FIC** possesses narrower optical bandgap of 1.48 eV, better π-π stacking, and its PBDB-T:**PTT-2FIC** blend film exhibited better morphology, and better hole and electron mobility. As a result, nonfullerene solar cells using PBDB-T:**PTT-2FIC** as the active layer achieved a decent PCE of 10.40%, with an open-circuit voltage (V_{OC}) of 0.87 V, a fill factor (FF) of 0.65, and a much higher short-circuit current (J_{SC}) of 18.26 mA/cm^2. Meanwhile, the PBDB-T:**PTT-IC** cells delivered a lower J_{SC} of 12.58 mA/cm^2 but a higher V_{OC} of 0.99 V, thus resulting in a PCE of 7.39% due to its wider optical bandgap of 1.58 eV and higher LUMO energy level. These results demonstrated that NFAs based on fused-ring donor core from fusing thieno[3,2-*b*]thiophenes with naphthalene *via* six-member-ring connection are promising for organic photovoltaic applications.

Keywords: organic solar cells; nonfullerene acceptors; naphthalene; six-member-ring; power conversion efficiency

1. Introduction

Organic solar cells (OSCs) have been re-sparkled by Zhan *et al.* since 2015 for the great discovery of fused-ring electron acceptors (FREAs), represented by ITIC [1], when fullerene derivatives acceptors such as phenyl-C_{61}/C_{71}-butyric acid methyl ester ($PC_{61}BM$/$C_{71}BM$) and indene-C_{70} bisadduct ($IC_{70}BA$) had become a bottle neck for further improvement on photovoltaic performance due to their drawbacks such as poor light absorption, limited tunability of chemical structures and energy levels, and morphology instability [2-6]. This breakthrough achievement has led to many impressive progresses on these nonfullerene acceptors (NFAs) and revived OSCs [7-11]. Generally, the NFAs take great advantages of acceptor-donor-acceptor (A-D-A) structure for the sake of efficient intramolecular charge transfer (ICT) between the donor and acceptor units, thus resulting in impressively wide absorption range and good light-harvesting capability [12-15]. Very recently, the power conversion efficiencies (PCEs) of OSCs have soared consistently up to 16~18% [16-29].

Among various donor cores in such A-D-A type NFAs, naphthalene has been adopted for replacing the benzene core of classic ITIC for improved PCEs in devices due to its rigid and planar structure with the diversity of synthetic controls, and endows its derivatives with large π-conjugation to reduce energetic disorder and induce strong intermolecular interactions [30-32]. Recently, a series of NFAs based on naphthalene core have been reported and exhibited promising PCEs of 5-11% [33-41]. However, in most of these NFAs, the naphthalene core had been always fused at ortho-positions leading to five-member-ring linkages, and the analogues with six-member-ring connection are far less common, even in all NFAs with spiral structures [40-44]. Bo *et al.* reported a dihydropyreno[1,2-*b*:6,7-*b′*]dithiophene-based NFA named PDT in 2019 demonstrating a PCE of 7.07% for its solar cells based on

PBDB-T:PDT. With additional thiophene bridges, the acceptor PDT-T can further improve the PCE up to 11% in devices [40]. Guo *et al.* reported one of their systematically studied polycyclic aromatic hydrocarbons (PAHs), namely DTN-IC-2Ph with a donor core of thiophene-fused naphthalene at 4,8 positions *via* six-member-ring connection, but gaining only a PCE of 5.45% with a low short-circuit current (J_{SC}) of 9.33 mA/cm^2 in their devices paired with PBDB-T as well [41]. It was noticed that only thiophenes were used to fuse with naphthalene core *via* five- or six-member ring connection, therefore, it will be interesting to use thieno[3,2-*b*]thiophene (TT) instead of thiophene fused on naphthalene and extend the conjugation of the donor segments.

In this work, we synthesized two A-D-A type NFAs **PTT-IC** and **PTT-2FIC**, whereas thieno[3,2-*b*]thiophenes were adopted for fusing onto naphthalene at 4,8 positions in bay-area *via* six-member ring linkages for the formation of the complete donor core dihydropyrenobisthieno[3,2-*b*]thiophene and then further to flanked with the electron withdrawing moieties 1,1-dicyanomethylene-3-indanone (IC) or 5,6-difluoro-1,1-dicyanomethylene-3-indanone (2FIC) as the end groups (Fig. 1). Two hexyloxy chains were introduced at the C2 and C6 positions of the naphthalene ring to not only enhance the solubility of target NFAs but also prevent from yielding five-member-ring connected isomers. The thermal, optical and electrochemical properties, charge carrier mobility, and photovoltaic performance of **PTT-IC** and **PTT-2FIC** were studied systematically. Compared with **PTT-IC**, fluorinated **PTT-2FIC** possessed red-shift absorption and narrower bandgaps, better stacking, and higher hole and electron mobilities. Under an illumination of AM 1.5G (100 mW/cm^2), solar cells using PBDB-T:**PTT-IC** or PBDB-T:**PTT-2FIC** as active layers have achieved decent PCEs up to 7.39% or 10.40%, respectively.

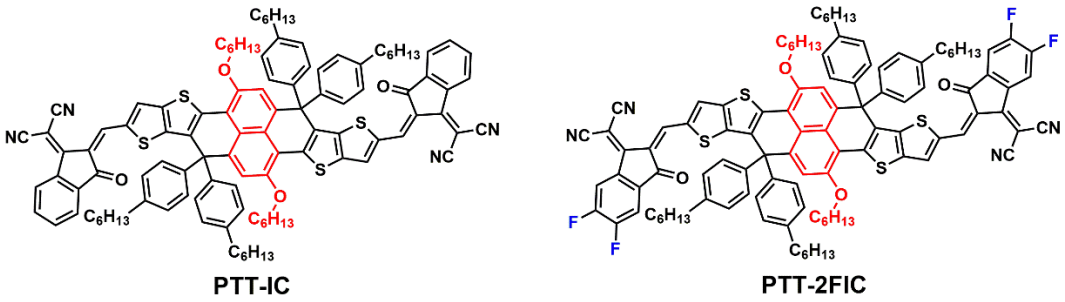

Fig. 1 Chemical structures of NFAs **PTT-IC** and **PTT-2FIC**.

2 Experimental section

2.1 Materials

All reagents were purchased from TCI Chemicals, Aladdin Co., Innochem Co., Derthon Co. and other commercial suppliers. 1,5-Dibromo-2,6-bis(hexyloxy)naphthalene (**2**), 2,2'-(2,6-bis(hexyloxy)naphthalene-1,5-diyl)bis(4,4,5,5-tetramethyl-1,3,2-dioxaborolane) (**3**), and ethyl 2-bromothieno[3,2-*b*]thiophene-3-carboxylate were prepared according to the literatures [45-47].

2.2 Syntheses

2.2.1 Synthesis of diethyl 2,2'-(2,6-bis(hexyloxy)naphthalene-1,5-diyl)bis(thieno[3,2-*b*]thiophene-3-carboxylate) (**4**).

To a mixture of compound **3** (557 mg, 0.96 mmol), ethyl 2-bromothieno[3,2-*b*]thiophene-3-carboxylate (699 mg, 2.4 mmol), toluene (50 mL), ethanol (30 mL) and 2 M potassium carbonate aqueous solution (20 mL), $Pd(PPh_3)_4$ (130 mg) was added under Ar. The mixture was heated to reflux for 24 h, and then

was poured into water and extracted with dichloromethane. The combined organic layer was dried over anhydrous $MgSO_4$ and then filtered. The solvent was removed and the residue was purified by column chromatography on silica gel using a mixture of petroleum ether/dichloromethane (1:2) as the eluent to give compound **4** as a light yellow solid (550 mg, 77%). ^{1}H NMR ($CDCl_3$, 500 MHz, δ/ppm): 7.63-7.59 (m, 2H), 7.50 (d, *J* = 5.3 Hz, 2H), 7.33 (d, *J* = 5.3 Hz, 2H), 7.21-7.18 (dd, *J* = 9.3, 5.3 Hz, 2H), 4.07 (q, *J* = 7.0 Hz, 4H), 4.00 (t, *J* = 6.4 Hz, 4H), 1.60-1.55 (m, 4H), 1.33-1.15 (m, 12H), 0.93 (t, *J* = 7.1 Hz, 6H), 0.77 (t, *J* = 5.8 Hz, 6H). ^{13}C NMR ($CDCl_3$, 125 MHz, δ/ppm): 161.89, 152.86, 147.56, 139.40, 137.39, 129.20, 128.10, 127.42, 123.88, 119.01, 117.25, 115.64, 69.66, 60.40, 31.32, 29.21, 25.46, 22.44, 13.87, 13.59. MS (MALDI-TOF, m/z): 748.280.

2.2.2 Synthesis of {[2,6-bis(hexyloxy)naphthalene-1,5-diyl]bis(thieno[3,2-*b*]thiophene-2,3-diyl)}bis(bis(4-hexylphenyl)methanol) (**5**).

To a solution of 1-bromo-4-hexylbenzene (1.29 g, 5.34 mmol) in 50 mL THF at -78 ℃, 2.1 mL of n-BuLi (2.5 M in hexane) was added dropwise under Ar. The mixture was stirred at -78 ℃ for 1 h, then compound **4** (667 mg, 0.89 mmol) in 20 mL THF was added by syringe. The mixture was stirred at room temperature overnight and then was poured into water. The mixture was extracted with ethyl acetate and the combined organic layer was dried over anhydrous $MgSO_4$. After removing the solvent, the orange residue was used in the next step without purification.

2.2.3 Synthesis of 5,12-bis(hexyloxy)-7,7,14,14-tetrakis(4-hexylphenyl)-7,14-dihydrodithieno[2,3-*d*:2′,3′-*d*′]pyreno[1,2-*b*:6,7-*b*′]dithiophene (**6**).

The crude compound **5** was dissolved in 50 mL dry toluene and 1.1 g Amberlyst 15

were added, then the mixture was refluxed for 6 h under Ar. After cooling to room temperature, the mixture was filtrated and the solvent was removed. The crude product was purified by column chromatography on silica gel using a mixture of petroleum ether/dichloromethane (10: 1) as the eluent to give compound **6** as a yellow solid (448 mg, 40%). ^{1}H NMR ($CDCl_3$, 400 MHz, δ/ppm): 7.18 (d, *J* = 5.2 Hz, 2H), 7.14 (d, *J* = 5.2 Hz, 2H), 7.06 (d, *J* = 8.3 Hz, 8H), 7.01 (d, *J* = 8.3 Hz, 8H), 6.96 (s, 2H), 3.97 (t, *J* = 6.7 Hz, 4H), 2.54 (t, *J* = 6.7 Hz, 8H), 1.89-1.82 (m, 4H), 1.56-1.52 (m, 8H), 1.49-1.44 (m, 4H), 1.33-1.26 (m, 32H), 0.91-0.84 (m, 18H). ^{13}C NMR ($CDCl_3$, 125 MHz, δ/ppm): 149.59, 143.37, 142.21, 141.20, 140.01, 139.16, 133.81, 133.37, 129.87, 127.83, 127.40, 123.07, 118.90, 118.10, 113.86, 69.60, 58.12, 35.40, 31.70, 31.61, 31.26, 29.33, 28.92, 25.80, 22.61, 22.54, 14.11, 14.07. MS (MALDI-TOF, m/z): 1269.57.

2.2.4 Synthesis of 5,12-bis(hexyloxy)-7,7,14,14-tetrakis(4-hexylphenyl)-7,14-dihydrodithieno[2,3-*d*:2′,3′-*d*′]pyreno[1,2-*b*:6,7-*b*′]dithiophene-2,9-dicarbaldehyde (**7**).

To a solution of compound **6** (240 mg, 0.19 mmol), 3.2 mL DMF, and 40 mL 1,2-dichloroethane at 0 °C was added $POCl_3$ (0.34 mL, 3.78 mmol) under Ar. The mixture was kept at 0 °C for 0.5 h, then was heated to 85 °C for 24 h. After cooling to room temperature, the mixture was poured into water (100 mL) and extracted with dichloromethane. After removal of the solvent, the crude product was purified by column chromatography on silica gel using a mixture of petroleum ether/dichloromethane (2: 1) as the eluent to give compound **7** as yellow solid (202 mg, 80%). ^{1}H NMR ($CDCl_3$, 500 MHz, δ/ppm): 9.83 (s, 2H), 7.86 (s, 2H), 7.04 (br, 16H), 7.00 (s, 2H), 4.00 (t, *J* = 6.6 Hz, 4H), 2.56 (t, *J* = 7.8 Hz, 8H), 1.89-1.83 (m, 4H), 1.56-1.54 (m, 8H), 1.52-1.46 (m, 4H), 1.34-1.26 (m, 32H), 0.91 (t, *J* = 6.8 Hz,

6H), 0.87 (t, *J* = 6.7 Hz, 12H). ^{13}C NMR ($CDCl_3$, 125 MHz, δ/ppm): 183.20, 150.83, 146.51, 144.57, 143.71, 142.38, 141.81, 139.71, 138.96, 133.84, 129.69, 129.07, 128.13, 122.78, 117.93, 112.95, 69.60, 58.06, 35.37, 31.67, 31.56, 31.16, 29.20, 28.94, 25.78, 22.58, 22.51, 14.10, 14.06. MS (MALDI-TOF, m/z): 1325.240.

2.2.5 Synthesis of **PTT-IC**.

To a solution of compound **7** (200 mg, 0.15 mmol), 1,1-dicyanomethylene-3-indanone (IC, 293 mg, 1.51 mmol) in 50 mL chloroform, 1 mL pyridine was added under Ar. The mixture was heated to reflux overnight. After cooling to room temperature, the mixture was poured into 150 mL methanol and filtered. The crude product was purified by column chromatography on silica gel using a mixture of petroleum ether/dichloromethane (1: 1) as the eluent to give **PTT-IC** as a brown-black solid (220 mg, 87%). ^{1}H NMR ($CDCl_3$, 500 MHz, δ/ppm): 8.74 (s, 2H), 8.63 (d, *J* = 7.0 Hz, 2H), 8.19 (s, 2H), 7.85-7.84 (m, 2H), 7.74-7.69 (m, 4H), 7.13 (s, 2H), 7.12 (br, 16H), 4.06 (t, *J* = 6.5 Hz, 4H), 2.58 (t, *J* = 7.5 Hz, 8H), 1.92-1.86 (m, 4H), 1.60-1.55 (m, 8H), 1.54-1.49 (m, 4H), 1.37-1.22 (m, 32H), 0.93 (t, *J* = 6.7 Hz, 6H), 0.81 (t, *J* = 6.9 Hz, 12H). ^{13}C NMR ($CDCl_3$, 125 MHz, δ/ppm): 187.39, 160.84, 154.21, 151.88, 144.87, 142.94, 142.16, 140.89, 140.16, 139.85, 138.18, 136.89, 134.76, 134.60, 134.11, 129.81, 128.36, 125.05, 123.55, 122.94, 122.26, 117.92, 114.88, 114.73, 113.34, 69.88, 68.43, 58.33, 35.49, 31.73, 31.58, 31.24, 29.68, 29.22, 29.03, 25.86, 22.59, 22.53, 14.06. MS (MALDI-TOF, m/z): 1677.568.

2.2.6 Synthesis of **PTT-2FIC**.

PTT-2FIC was synthesized by following the same procedures for **PTT-IC**. Compound **7** (200 mg, 0.15 mmol) and 5,6-difluoro-1,1-dicyanomethylene-3-indanone (2FIC, 208 mg, 0.90 mmol) were used

as starting materials. **PTT-2FIC** was obtained as a blue-black solid (237 mg, 90%). ^{1}H NMR ($CDCl_3$, 500 MHz, δ/ppm): 8.74 (s, 2H), 8.49 (dd, *J* = 9.8, 6.5 Hz, 2H), 8.20 (s, 2H), 7.60 (t, *J* = 7.5 Hz, 2H), 7.12 (s, 2H), 7.10 (br, 16H), 4.07 (t, *J* = 6.5 Hz, 4H), 2.58 (t, *J* = 7.6 Hz, 8H), 1.94-1.88 (m, 4H), 1.61-1.56 (m, 8H), 1.54-1.49 (m, 4H), 1.37-1.23 (m, 32H), 0.95-0.92 (m, 6H), 0.84-0.81 (m, 12H). ^{13}C NMR ($CDCl_3$, 125 MHz, δ/ppm): 185.12, 158.67, 155.08, 153.13, 152.06, 145.07, 143.85, 142.24, 141.95, 141.00, 140.00, 138.40, 136.60, 134.59, 134.44, 129.74, 128.38, 122.86, 121.09, 117.81, 114.84, 114.67, 114.50, 114.31, 113.21, 112.46, 112.31, 69.85, 68.76, 58.28, 35.48, 31.75, 31.57, 31.30, 29.18, 29.04, 25.87, 22.60, 22.54, 14.08. MS (MALDI-TOF, *m*/*z*): 1749.444.

3. Results and Discussion

3.1 Synthesis and characterization

As shown in Scheme 1, the synthetic routes of **PTT-IC** and **PTT-2FIC** are different from the method reported by Bo *et al* [40]. Firstly, 1,5-dibromo-2,6-bis(hexyloxy)naphthalene (**2**) and 2,2'-(2,6-bis(hexyloxy)naphthalene-1,5-diyl)bis(4,4,5,5-tetramethyl-1,3,2-dioxaborolane) (**3**) were synthesized according to the literature [45,46]. Compound **3** was reacted with ethyl 2-bromothieno[3,2-*b*]thiophene-3-carboxylate *via* the Suzuki coupling reaction to produce diethyl 2,2'-(2,6-bis(hexyloxy)naphthalene-1,5-diyl)bis(thieno[3,2-*b*]thiophene-3-carboxylate) (**4**), which was then treated with (4-hexylphenyl)lithium to afford tertiary alcohol intermediate **5**. Subsequently, compound **5** was converted to dialdehyde compound **7** *via* Amberlyst 15 assisted ring-closure reaction and Vilsmeier-Haack formylation reaction. Finally, **PTT-IC** and **PTT-2FIC** were obtained by Knoevenagel condensation reaction between compound **7** and end-capping group IC or 2FIC,

respectively. The intermediates and the two targeted NFAs were well characterized by ^{1}H NMR, ^{13}C NMR, and MS (Fig. S1-S8). These two NFAs possess good solubility in common organic solvents such as dichloromethane, chloroform, and chlorobenzene for solution process. As shown in Fig. S9, **PTT-IC** and **PTT-2FIC** show good thermostability with decomposition temperatures (T_d, 5% wt loss) of 354 and 337 °C, respectively.

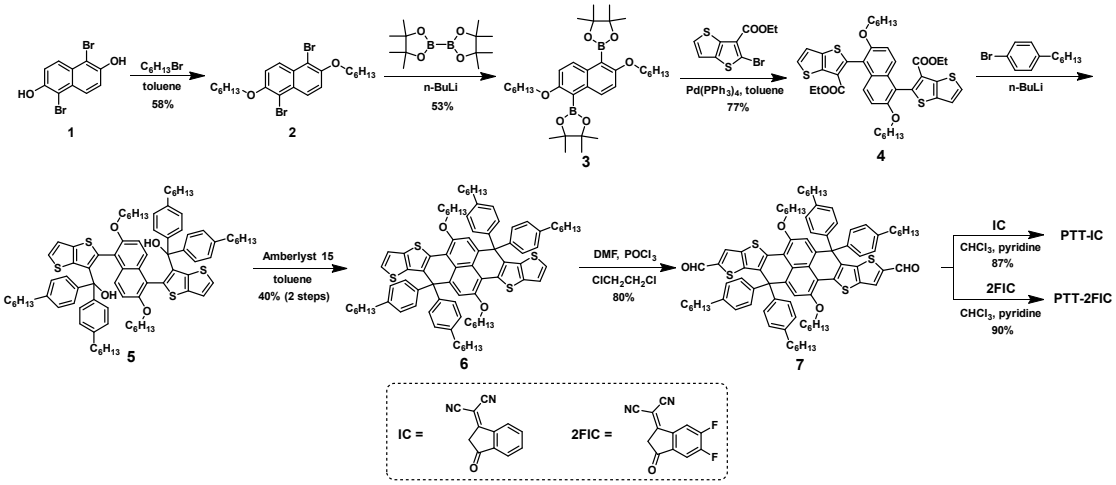

Scheme 1 Synthetic routes for **PTT-IC** and **PTT-2FIC**.

3.2 Optical properties

The ultraviolet-visible (UV-vis) absorption spectra of **PTT-IC** and **PTT-2FIC** in chloroform solutions and as films are shown in Fig. 2a, with corresponding data summarized in Table 1. In dilute chloroform solution (10^{-5} M), **PTT-IC** and **PTT-2FIC** exhibited good absorption in the 600-750 nm region with absorption peak at 692 and 707 nm, respectively. It is noteworthy that **PTT-2FIC** possessed ~50% higher molar extinction coefficient than that of **PTT-IC** (1.49×10^5 M^{-1} cm^{-1} *vs* 1.02×10^5 M^{-1} cm^{-1}), which is beneficial for achieving higher external quantum efficiency (EQE). From solution to film, **PTT-IC** showed a red-shift of 18 nm with λ_{max} of 710 nm. Interestingly, the absorption peak of **PTT-2FIC** was 749 nm with remarkable

red-shift of 42 nm, which suggests much better π-π stacking for higher charge carrier transport. The absorption onsets of **PTT-IC** and **PTT-2FIC** are located at 786 and 836 nm, respectively. According to $E_g^{opt} = 1240/\lambda_{onset}$, the optical bandgap ($E_g^{opt}$) of **PTT-IC** and **PTT-2FIC** were calculated as 1.58 and 1.48 eV, respectively. Compared with **PTT-IC**, **PTT-2FIC** exhibited much red-shift and much better complementary absorption spectrum with PBDB-T. These results all reveal that **PTT-2FIC**-based devices could afford much higher photocurrents. In addition, the optical bandgap of **PTT-2FIC** is much narrower than other naphthalene core based NFAs fusing *via* five-member-ring [33-35], probably due to the extended conjugation and more effective conjugation pathway of **PTT-2FIC** [44,48-51].

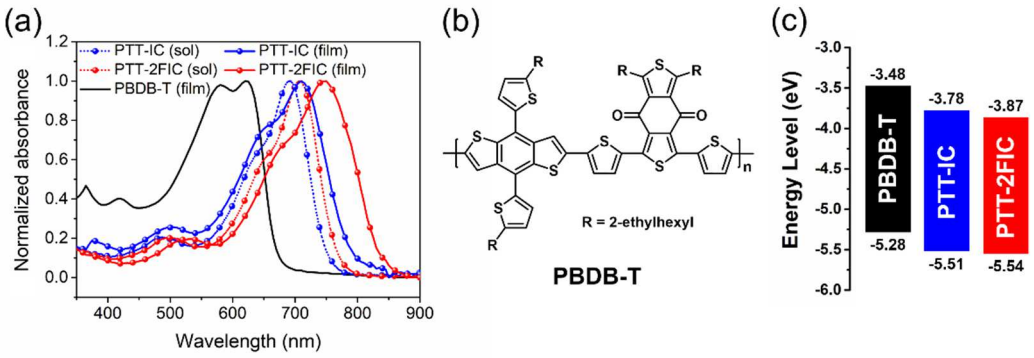

Fig. 2 Absorption spectra of **PTT-IC** and **PTT-2FIC** (a), chemical structure of PBDB-T (b), and energy level diagrams (c).

Table 1 Optical and electrochemical properties of **PTT-IC** and **PTT-2FIC**.

NFAs	λ_{sol} [nm]	λ_{film} [nm]	λ_{onset} [nm]	E_g^{opt} [eV][a]	E_{ox}^{on} [V]	E_{red}^{on} [V]	HOMO [eV][b]	LUMO [eV][b]	HOMO [eV][c]	LUMO [eV][c]
PTT-IC	692	710	786	1.58	0.71	-1.02	-5.51	-3.78	-5.23	-3.14
PTT-2FIC	707	749	836	1.48	0.74	-0.93	-5.54	-3.87	-5.35	-3.29

[a] $E_g^{opt} = 1240/\lambda_{onset}$.

[b] HOMO = -(E_{ox}^{on} + 4.8) eV, LUMO = -(E_{red}^{on} + 4.8) eV.

[c] Calculated from DFT.

3.3 Electrochemical properties and theoretical calculations

As shown in Fig. 3, cyclic voltammetry (CV) was used to investigate the electrochemical properties of these nonfullerene acceptors, and all potentials were calibrated against ferrocene/ferrocenium (Fc/Fc^+) redox couple. The onset of oxidation potential (E_{ox}^{on}) of **PTT-IC** and **PTT-2FIC** were observed at 0.71 V and 0.74 V, corresponding to the HOMO energy level at -5.51 eV and -5.54 eV, respectively. The onset of reduction potential (E_{red}^{on}) of **PTT-IC** and **PTT-2FIC** were observed at -1.02 V and -0.93 V, corresponding to the LUMO energy level at -3.78 eV and -3.87 eV, respectively. **PTT-2FIC** exhibited slightly lowered HOMO and much lowered LUMO energy levels, and eventually narrower electrochemical bandgap (1.67 eV) compared to non-fluorinated **PTT-IC** (1.73 eV). These trends are also consistent well with the optical results. The energy levels of **PTT-IC** and **PTT-2FIC** exhibited good match with the well-known polymer donor PBDB-T (Fig. 2c), and higher LUMO energy level of **PTT-IC** could endow its devices with higher open-circuit voltage (V_{OC}) [52-54].

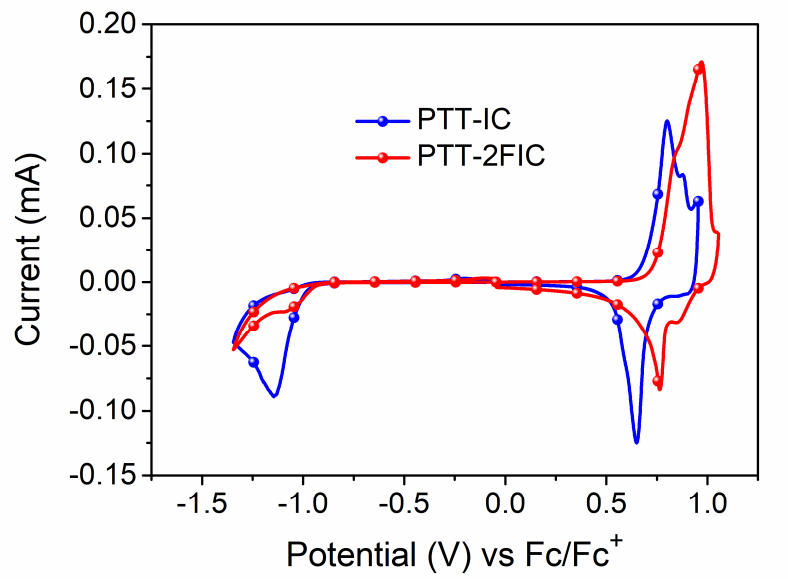

Fig. 3 Cyclic voltammograms of **PTT-IC** and **PTT-2FIC** measured in 0.1 M Bu_4NPF_6 acetonitrile solution at a scan rate of 100 mV/s.

Density functional theory (DFT) calculations at the B3LYP/6-31G(d,p) level were carried out to investigate optimal geometric configurations and molecular frontier orbitals for these two NFAs (Fig. S10). There found two major conformers for **PTT-IC** and **PTT-2FIC**, respectively, and then Boltzmann distribution calculation was further performed [55]. As shown in Table S1, for **PTT-IC**, the two conformers are calculated to have a population of 87.89% *vs* 12.11% by the Boltzmann distribution law, the predominant **PTT-IC***a* being 4.908 kJ/mol (1.17 kcal/mol) lower in Gibbs free energy in gas phase than its conformer **PTT-IC***b*. For **PTT-2FIC**, the Boltzmann distribution reveals that the predominant conformer (**PTT-2FIC***a*) takes up 95.06% and is 7.324 kJ/mol (1.75 kcal/mol) lower in Gibbs free energy in gas than **PTT-2FIC***b*. Taken solvents such as chloroform into consideration, the Boltzmann population of the predominant conformer will become 98.65% and 99.57% for **PTT-IC***a* and **PTT-2FIC***a*, respectively. In both cases, the calculated Boltzmann distribution results are consistent with the conformational preference as evidenced by

the crystal studies in the literature [56,57]. However, the conformational effect on the calculated HOMO and LUMO energies is negligible (Fig. S10). The calculated HOMO and LUMO levels at the B3LYP-D3(BJ)/6-31G(d,p) level are -5.23/-3.14 eV and -5.35/-3.29 eV for **PTT-IC** and **PTT-2FIC**, respectively, which showed the same trends with the values evaluated in the CV measurement. Just as the reported PDT with six-member-rings [40], **PTT-IC** and **PTT-2FIC** both exhibited similar twisted molecular conformation. For both NFAs, the HOMOs are mostly localized on the electron-donating units, while the LUMOs are delocalized on the terminal electron-withdrawing units, suggesting effective ICT effect [58].

TD-DFT calculation based on the optimized molecular geometries at the CAM-B3LYP-D3(BJ)/6-31G(d,p) level suggests the lowest excitations from the ground state (S_0) to the excited state (S_1) correspond to π-π* transitions and are all a consequence of combined contributions from several pairs of molecular orbitals, with around 70% dominated by the HOMO→LUMO transitions (Table S2). As shown in Table S3, electron-hole analysis of the transitions from the ground state to the excited states reveals that these NFAs feature high overlap of well distributed holes and electrons of the transitions, where the $S_0 \rightarrow S_1$ transitions have the highest oscillator strengths compared to other transitions of the same systems. The excited-state vertical transition energies show similar trends to the HOMO-LUMO gaps. That is to say, the introduction of fluorine atoms on the NFA molecules led to lowered HOMO and much lowered LUMO energy levels, therefore also resulting in narrower bandgaps, as many other reported fluorinated NFAs [5,8].

3.4 Photovoltaic properties

In order to investigate the photovoltaic performance of **PTT-IC** and **PTT-2FIC**, OSCs with a configuration of ITO/PEDOT:PSS/Active layer/PFN-Br/Al were

fabricated, and the widely used polymer PBDB-T was chosen as electron donor material for the above-mentioned reasons. Under an illumination of AM 1.5 G (100 mW/cm^2), PBDB-T:**PTT-IC** cells exhibited a PCE of 7.39%, with a V_{OC} of 0.99 V, a J_{SC} of 12.58 mA/cm^2 and a fill factor (FF) of 0.59 (Fig. 4a and Table 2). Meanwhile, solar cells using PBDB-T:**PTT-2FIC** as the active layer achieved a better PCE of 10.40%, with a V_{OC} of 0.87 V, and a FF of 0.65, and a much higher J_{SC} of 18.26 mA/cm^2. As far as we know, this PCE is among the highest value for OSCs based on naphthalene-core NFAs. The high V_{OC} of 0.99 V for PBDB-T:**PTT-IC** cells could originate from the higher LUMO energy level, as V_{OC} is roughly proportional to the difference between the HOMO energy levels of the donor material (PBDB-T) and the LUMO energy levels of the acceptor materials (**PTT-IC** or **PTT-2FIC**) [52]. The photocurrent density versus effective voltage (J_{ph}-V_{eff}) curves (Fig. S11) showed that under short-circuit condition, the exciton dissociation efficiency of PBDB-T:**PTT-IC** and PBDB-T:**PTT-2FIC** solar cells are 94% and 96%, respectively. These results were consistent with the higher J_{SC} in OSCs based on PBDB-T:**PTT-2FIC**.

PBDB-T:**PTT-2FIC** cell showed ~50% higher J_{SC} than that of PBDB-T:**PTT-IC** cells, which was confirmed by the EQE. As shown in Fig. 4b, PBDB-T:**PTT-2FIC** cell possessed ~10% higher and ~50 nm broader EQE response than that of PBDB-T:**PTT-IC** cell, consisting well with the absorption spectra of blend films (Fig. S12). The EQE spectra exhibited obvious peaks at ~710 nm for PBDB-T:**PTT-IC** cell and ~760 nm for PBDB-T:**PTT-2FIC** cell, which are consistent with the absorption of **PTT-IC** and **PTT-2FIC**, respectively. The integrated currents from EQE spectra are 10.42 and 15.40 mA/cm^2 for these two cells, and these values agree well with those from *J*-*V* measurements.

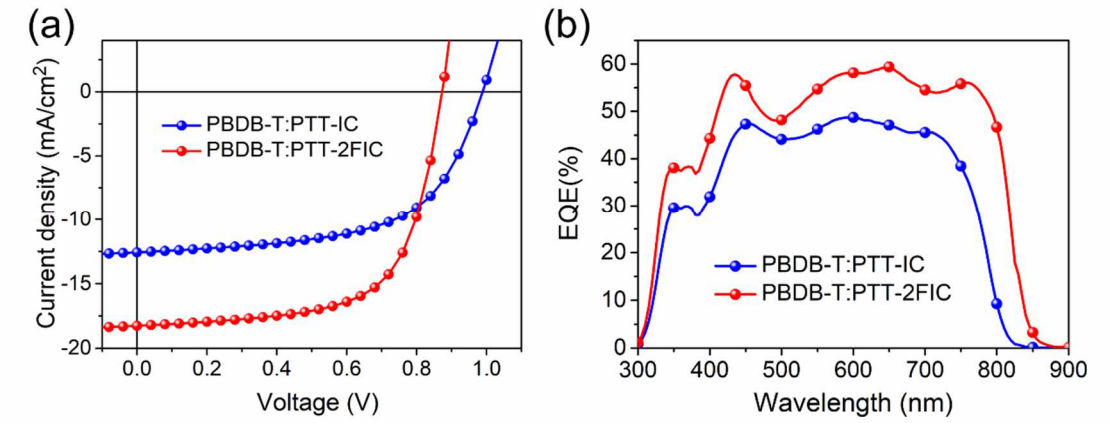

Fig. 4 *J-V* curves (a) and EQE spectra (b) of PBDB-T:NFA solar cells.

Table 2 Photovoltaic performance of PBDB-T:NFA solar cells.

Active layer	V_{oc} [V]	J_{sc} [mA/cm^2]	FF	PCE [%]
PBDB-T:PTT-IC	0.99	12.58	0.59	7.39
	(0.99±0.01)	(12.72±0.15)	(0.56±0.03)	(7.10±0.29)
PBDB-T:PTT-2FIC	0.87	18.26	0.65	10.40
	(0.87±0.01)	(17.87±0.38)	(0.64±0.01)	(9.98±0.42)

[a] The averaged values of device parameters with standards deviation from ~10 cells are included in parentheses.

3.5 PL Quenching

Steady-state photoluminescence (PL) measurements were taken to study charge transfer between donors and acceptors, and the PL spectra (excited at 532 nm) are shown in Fig. 5 and Fig. S13. For the PL spectra of films of pure donor and its blend films with the two NFAs (**PTT-IC** and **PTT-2FIC**), PBDB-T alone shows a broad emission between 680 to 750 nm, then was almost quenched to 63% and 42% of its original emission when mixing with **PTT-IC** and **PTT-2FIC**, respectively. This

clearly indicates efficient charge transfer from PBDB-T to these NFAs. However, comparing with the quenching ratio of either 98% or 92% for **PTT-IC** or **PTT-2FIC**, such significant inefficient quenching strongly indicates effective energy transfer from the donor PBDB-T to the two acceptors in their respective blend films, which can be primarily confirmed by the effective overlapping between the strong emission of PBDB-T (680-750 nm) and the predominant absorption of either **PTT-IC** or **PTT-2FIC** (550-800 nm or 600-850 nm) [59]. The PL of **PTT-IC** and **PTT-2FIC** films show emission peaks at 800 nm and 825 nm, respectively. Compared to the PL spectra of pristine acceptor films, PBDB-T:**PTT-2FIC** exhibits nearly complete PL quenching (98%), suggesting a good mixture between donor and acceptor and efficient charge transfer at PBDB-T:**PTT-2FIC** interface, while reduced PL quenching efficiency was observed in PBDB-T:**PTT-IC** blend [60,61]. The incomplete PL quenching (92%) is consistent with the smaller J_{SC} in PBDB-T:**PTT-IC** device and larger phase size in corresponding morphology.

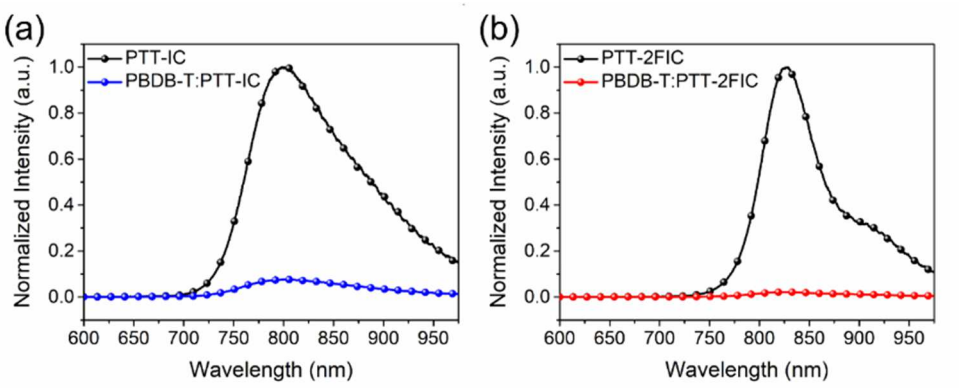

Fig. 5 PL spectra (excitation wavelength of 532 nm) of pure **PTT-IC** and blend film (a) and pure **PTT-2FIC** and blend film (b).

3.6 Mobilities and morphology

We also used the space-charge limited current (SCLC) method to investigate the reasons for the better photovoltaic performance of PBDB-T:**PTT-2FIC** cell (Fig. S14). It was found that PBDB-T:**PTT-2FIC** based devices exhibited the hole and electron mobilities of 6.62×10^{-4} and 6.69×10^{-4} cm^2 V^{-1} s^{-1}, respectively. While, the hole and electron mobilities of PBDB-T:**PTT-IC** blend film were just 1.09×10^{-4} and 4.68×10^{-5} cm^2 V^{-1} s^{-1}. The much higher and balanced charge carrier mobilities could contribute to the higher J_{SC} and FF for the corresponding PBDB-T:**PTT-2FIC** cell [62-64].

As shown in Fig. 6, atomic force microscopy (AFM) was used to study the morphology of the blend films. When compared with PBDB-T:**PTT-IC** blend films with root mean square (RMS) roughness of 3.69 nm, PBDB-T:**PTT-2FIC** film present finer nano-sized domains and smoother surface with the reduced RMS roughness of 2.10 nm for slightly shorter fibrils. Moreover, the smaller domain size as indicated in PBDB-T:**PTT-2FIC** film are beneficial for charge separation and thus higher photocurrents [52,53], therefore, enhanced photovoltaic performance for PBDB-T:**PTT-2FIC** cell can be expected.

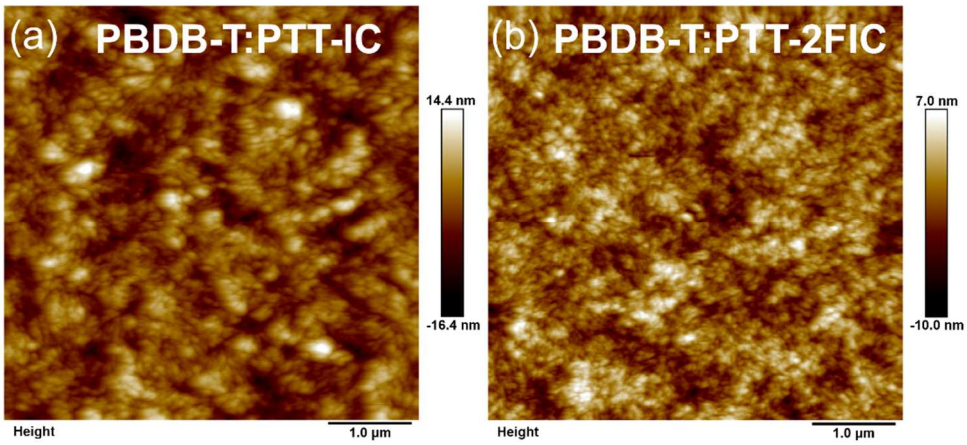

Fig. 6 AFM height images of PBDB-T:**PTT-IC** (a) and PBDB-T:**PTT-2FIC** blend

films (b).

4. Conclusions

In conclusion, we have developed an octacyclic core unit dihydropyrenobisthieno[3,2-*b*]thiophene by fusing thieno[3,2-*b*]thiophenes at the bay position of naphthalene *via* two six-member-ring connection. When combined with electron withdrawing moieties IC or 2FIC, two NFAs **PTT-IC** and **PTT-2FIC** have been synthesized, respectively. Non-fluorinated **PTT-IC** possessed an E_g^{opt} of 1.58 eV. Meanwhile, fluorinated **PTT-2FIC** exhibited narrower E_g^{opt} of 1.48 eV, better intermolecular stacking. Furthermore, the higher and balanced hole and electron mobilities, and optimized morphology of the PBDB-T:**PTT-2FIC** blend film endowed corresponding OSCs with enhanced photocurrent of 18.26 mA/cm^2 and higher FF of 0.65, thus resulting in a much higher PCE of 10.40%. In contrast, the control devices based on PBDB-T:**PTT-IC** just achieved a PCE of 7.39%. Our results demonstrated that naphthalene fused with thieno[3,2-*b*]thipohenes *via* six-member-ring connection as donor core for NFAs is a promising strategy to develop efficient NFAs and worth for further investigation.

Acknowledgements

S.D. and N.Y. contributed equally to this work. J.C. acknowledges financial support from the National Natural Science Foundation of China (21604021), China Scholarship Council (CSC, 201808430041), Hunan Provincial Natural Science Foundation (2018JJ3141), and School of Materials Science and Engineering, Jiangsu Engineering Laboratory of Light-Electricity-Heat Energy-Converting Materials and Applications. N.Y. and F.Z. acknowledge funding from the Knut and Alice

Wallenberg Foundation under Contract 2016.0059, the Swedish Government Research Area in Materials Science on Functional Materials at Linköping University (Faculty Grant SFO-Mat-LiU 200900971), and China Scholarship Council (CSC, 201708370115). D. Y. thanks the financial support Sino-Danish Centre for Education and Research (SDC). W.Z. appreciates support from the China Scholarship Council (201908440047), NSFC project (11272093), Guangzhou Municipal Science and Technology Bureau (201804010501, 201904010381), Department of Education of Guangdong Province (2018GKTSCX041, 2017GKQNCX005), Department of Science and Technology of Guangdong Province (2016A010103046), and the Open Fund of the State Key Laboratory of Luminescent Materials and Devices (South China University of Technology, 2020-skllmd-07). N.W. acknowledges financial support from China Scholarship Council (CSC, 201808620028). E.W. thanks the Swedish Research Council (2015-04853, 2016-06146, 2019-04683), the Swedish Research Council Formas, and the Wallenberg Foundation (2017.0186, 2016.0059) for financial support.

References

[1] Lin Y, Wang J, Zhang Z-G, Bai H, Li Y, Zhu D, et al. An electron acceptor challenging fullerenes for efficient polymer solar cells. Adv Mater 2015;27:1170-4.

[2] Cui C, Li Y, Li Y. Fullerene derivatives for the applications as acceptor and cathode buffer layer materials for organic and perovskite solar cells. Adv Energy Mater 2017;7:1601251.

[3] Xiao Z, Geng X, He D, Jia X, Ding L. Development of isomer-free fullerene bisadducts for efficient polymer solar cells. Energy Environ Sci 2016;9:2114-21.

[4] Yan C, Barlow S, Wang Z, Yan H, Jen AK-Y, Marder SR, et al. Non-fullerene

acceptors for organic solar cells. Nat Rev Mater 2018;3:18003.

[5] Cheng P, Li G, Zhan X, Yang Y. Next-generation organic photovoltaics based on non-fullerene acceptors. Nat Photonics 2018;12:131-42.

[6] Hou J, Inganäs O, Friend RH, Gao F. Organic solar cells based on non-fullerene acceptors. Nat Mat 2018;17:119-28.

[7] Lin Y, Zhang Z-G, Bai H, Wang J, Yao Y, Li Y, et al. High-performance fullerene-free polymer solar cells with 6.31% efficiency. Energy Environ Sci 2015;8:610-6.

[8] Xiao Z, Yang S, Yang Z, Yang J, Yip H-L, Zhang F, et al. Carbon-oxygen-bridged ladder-type building blocks for highly efficient nonfullerene acceptors. Adv Mater 2019;31:1804790.

[9] Yuan J, Zhang Y, Zhou L, Zhang G, Yip H-L, Lau T-K, et al. Single-junction organic solar cell with over 15% efficiency using fused-ring acceptor with electron-deficient core. Joule 2019;3:1140-51.

[10] Zhou R, Jiang Z, Yang C, Yu J, Feng J, Adil MA, et al. All-small-molecule organic solar cells with over 14% efficiency by optimizing hierarchical morphologies. Nat Commun 2019;10:5393.

[11] Luo Z, Liu T, Wang Y, Zhang G, Sun R, Chen Z, et al. Reduced energy loss enabled by a chlorinated thiophene-fused ending-group small molecular acceptor for efficient nonfullerene organic solar cells with 13.6% efficiency. Adv Energy Mater 2019;9:1900041.

[12] Fan H. Zhu X. Development of small-molecule materials for high-performance

organic solar cells. Sci China Chem 2015;58:922-36.

[13] Li C, Fu H, Xia T, Sun Y. Asymmetric nonfullerene small molecule acceptors for organic solar cells. Adv Energy Mater 2019;9:1900999.

[14] Fan Q, Su W, Chen S, Kim W, Chen X, Lee B, et al. Mechanically robust all-polymer solar cells from narrow band gap acceptors with hetero-bridging atoms. Joule 2020;4:658-72.

[15] Zhang Z, Feng L, Xu S, Liu Y, Peng H, Zhang Z-G, et al. A new electron acceptor with *meta*-alkoxyphenyl side chain for fullerene-free polymer solar cells with 9.3% efficiency. Adv Sci 2017;4:1700152.

[16] Meng L, Zhang Y, Wan X, Li C, Zhang X, Wang Y, et al. Organic and solution-processed tandem solar cells with 17.3% efficiency. Science 2018;361:1094-8.

[17] Liu Q, Jiang Y, Jin K, Qin J, Xu J, Li W, et al. 18% Efficiency organic solar cells. Sci Bull 2020;65:272-5.

[18] Xiong J, Jin K, Jiang Y, Qin J, Wang T, Liu J, et al. Thiolactone copolymer donor gifts organic solar cells a 16.72% efficiency. Sci Bull 2019;64:1573-6.

[19] Cui Y, Yao H, Hong L, Zhang T, Tang Y, Lin B, et al. 17% efficiency organic photovoltaic cell with superior processability. Natl Sci Rev 2019; DOI: 10.1093/nsr/nwz200.

[20] Jiang K, Wei Q, Lai JYL, Peng Z, Kim HK, Yuan J, et al. Alkyl chain tuning of small molecule acceptors for efficient organic solar cells. Joule 2019;3:3020-33

[21] Xu X, Feng K, Bi Z, Ma W, Zhang G, Peng Q. Single-junction polymer solar

cells with 16.35% efficiency enabled by a Platinum(II) complexation strategy. Adv Mater 2019;31:1901872.

[22] Sun H, Liu T, Yu J, Lau T-K, Zhang G, Zhang Y, et al. A monothiophene unit incorporating both fluoro and ester substitution enabling high-performance donor polymers for non-fullerene solar cells with 16.4% efficiency. Energy Environ Sci 2019;12:3328-37.

[23] Yan T, Song W, Huang J, Peng R, Huang L, Ge Z. 16.67% rigid and 14.06% flexible organic solar cells enabled by ternary heterojunction strategy. Adv Mater 2019;31:1902210.

[24] Su D, Pan M-A, Liu Z, Lau T-K, Li X, Shen F, et al. A trialkylsilylthienyl chain-substituted small-molecule acceptor with higher LUMO level and reduced band gap for over 16% efficiency fullerene-free ternary solar cells. Chem Mater 2019;31:8908-17.

[25] Sun C, Qin S, Wang R, Chen S, Pan F, Qiu B, et al. High efficiency polymer solar cells with efficient hole transfer at zero highest occupied molecular orbital offset between methylated polymer donor and brominated acceptor. J Am Chem Soc 2020;142:1465-74.

[26] An Q, Ma X, Gao J, Zhang F. Solvent additive-free ternary polymer solar cells with 16.27% efficiency. Sci Bull 2019;64:504-6.

[27] Fan B, Zhang D, Li M, Zhong W, Zeng Z, Ying L, et al. Achieving over 16% efficiency for single-junction organic solar cells. Sci China Chem 2019;62:746-52.

[28] Luo Z, Ma R, Liu T, Yu J, Xiao Y, Sun R, et al. Fine-tuning energy levels via

asymmetric end groups enables polymer solar cells with efficiencies over 17%. Joule 2020;4:1236-47.

[29] Xie G, Zhang Z, Su Z, Zhang X, Zhang J. 16.5% efficiency ternary organic photovoltaics with two polymer donors by optimizing molecular arrangement and phase separation. Nano Energy 2020;69:104447.

[30] Ma Y, Zheng Q, Wang L, Cai D, Tang C, Wang M, et al. Improving the photovoltaic performance of ladder-type dithienonaphthalene-containing copolymers through structural isomerization. J Mater Chem A 2014;2:13905-15.

[31] Osaka I, Takimiya K. Naphthobischalcogenadiazole conjugated polymers: emerging materials for organic electronics. Adv Mater 2017;29:1605218.

[32] Qian L, Cao J, Ding L. A hexacyclic ladder-type building block for high-performance D-A copolymers. J Mater Chem A 2015;3:24211-4.

[33] Zhu J, Wu Y, Rech J, Wang J, Liu K, Li T, et al. Enhancing the performance of a fused-ring electron acceptor via extending benzene to naphthalene. J Mater Chem C 2018;6:66-71.

[34] Zhu J, Ke Z, Zhang Q, Wang J, Dai S, Wu Y, et al. Naphthodithiophene-based nonfullerene acceptor for high-performance organic photovoltaics: effect of extended conjugation. Adv Mater 2018;30:1704713.

[35] Ma Y, Zhang M, Yan Y, Xin J, Wang T, Ma W, et al. Ladder-type dithienonaphthalene-based small-molecule acceptors for efficient nonfullerene organic solar cells. Chem Mater 2017;29:7942-52.

[36] Feng H, Yi Y-Q-Q, Ke X, Zhang Y, Wan X, Li C, et al. Synergistic modifications

of side chains and end groups in small molecular acceptors for high efficient non-fullerene organic solar cells. Sol RRL 2018;2:1800053.

[37] Zhang J, Yan C, Wang W, Xiao Y, Lu X, Barlow S, et al. Panchromatic ternary photovoltaic cells using a nonfullerene acceptor synthesized using C-H functionalization. Chem Mater 2018;30:309-13.

[38] Yi Y-Q-Q, Feng H, Chang M, Zhang H, Wan X, Li C, et al. New small-molecule acceptors based on hexacyclic naphthalene(cyclopentadithiophene) for efficient non-fullerene organic solar cells. J Mater Chem A 2017;5:17204-10.

[39] Zheng R, Guo Q, Hao D, Zhang C, Xue W, Huang H, et al. Naphthalene core-based noncovalently fused-ring electron acceptors: effects of linkage positions on photovoltaic performances. J Mater Chem C 2019;7:15141-7.

[40] Jiang P, Lu H, Jia Q-Q, Feng S, Li C, Li H-B, et al. Dihydropyreno[1,2-*b*:6,7-*b'*]dithiophene based electron acceptors for high efficiency as-cast organic solar cells. J Mater Chem A 2019;7:5943-8.

[41] Wang Y, Liu B, Koh CW, Zhou X, Sun H, Yu J, et al. Facile synthesis of polycyclic aromatic hydrocarbon (PAH)-based acceptors with fine-tuned optoelectronic properties: toward efficient additive-free nonfullerene organic solar cells. Adv Energy Mater 2019;9:1803976.

[42] Yao Z, Liao X, Gao K, Lin F, Xu X, Shi X, et al. Dithienopicenocarbazole-based acceptors for efficient organic solar cells with optoelectronic response over 1000 nm and an extremely low energy loss. J Am Chem Soc 2018;140:2054-7.

[43] Lu B, Xiao Y, Li T, Liu K, Lu X, Lian J, et al. Z-Shaped fused-chrysene electron

acceptors for organic photovoltaics. ACS Appl Mater Interfaces 2019;11:33006-11.

[44] Liu S, Su W, Zou X, Du X, Cao J, Wang N, et al. The role of connectivity in significant bandgap narrowing for fused-pyrene based non-fullerene acceptors toward high-efficiency organic solar cells. J Mater Chem A 2020;8:5995-6003.

[45] Yamaguchi I, Kondo A. Chemical properties and self-assembled-ordered structures of π-conjugated cooligomers consisted of 2,6-dialkoxynaphthalene-1,5-diyl, 2,1,3-benzothiadiazole-4,7-diyl, and 1,4-phenylenediethynylene units. Polym Bull 2018;75:1635-50.

[46] Nehls BS, Füldner S, Preis E, Farrell T, Scherf U. Microwave-assisted synthesis of 1,5- and 2,6-linked naphthylene-based ladder polymers. Macromolecules 2005;38:687-94.

[47] He D, Qian L, Ding L. A pentacyclic building block containing an azepine-2,7-dione moiety for polymer solar cells. Polym Chem 2016;7:2329-32.

[48] Li X, Yan T, Bin H, Han G, Xue L, Liu F, et al. Insertion of double bond π-bridges of A-D-A acceptors for high performance near-infrared polymer solar cells. J Mater Chem A 2017;5:22588-97.

[49] Cao J, Zuo C, Yu J, Tang Z. D-A copolymers based on lactam acceptor unit and thiophene derivatives for efficient polymer solar cells. Dyes Pigments 2017;139:201-7.

[50] Jia B, Dai S, Ke Z, Yan C, Ma W, Zhan X, Breaking 10% efficiency in semitransparent solar cells with fused-undecacyclic electron acceptor. Chem Mater 2018;30:239-45.

[51] Wang H, Cao J, Yu J, Zhang Z, Geng R, Yang L, et al. Molecular engineering of central fused-ring cores of non-fullerene acceptors for high-efficiency organic solar cells. J Mater Chem A 2019;7:4313-33.

[52] Cao J, Liao Q, Du X, Chen J, Xiao Z, Zuo Q, Ding L. A pentacyclic aromatic lactam building block for efficient polymer solar cells. Energy Environ Sci 2013;6:3224-8.

[53] Gu Z, Guo J, Hao R, Lin Z, Qian Y, Ma C, et al. An efficient strategy to supervise absorption, mobility, morphology of photovoltaic molecule by inserting a D-A unit. Dyes Pigments 2019;166:515-22.

[54] Xu S, Feng L, Yuan J, Cimrová V, Chen G, Zhang Z-G, et al. New *m*-alkoxy-*p*-fluorophenyl difluoroquinoxaline based polymers in efficient fullerene solar cells with high fill factor. Org Electron 2017;50:7-15.

[55] Lu T, Manzetti S. Wavefunction and reactivity study of benzo[a]pyrene diol epoxide and its enantiomeric forms. Struct Chem 2014;25:1521-33.

[56] Han G, Guo Y, Song X, Wang Y, Yi Y. Terminal π-π stacking determines three-dimensional molecular packing and isotropic charge transport in an A-π-A electron acceptor for non-fullerene organic solar cells. J Mater Chem C 2017;5:4852-7.

[57] Lai H, Chen H, Zhou J, Qu J, Chao P, Liu T, et al. Isomer-free: precise positioning of chlorine-induced interpenetrating charge transfer for elevated solar conversion. iScience, 2019;17:302-14.

[58] Shi X, Zuo L, Jo SB, Gao K, Lin F, Liu F, et al. Design of a highly crystalline

low-band gap fused-ring electron acceptor for high-efficiency solar cells with low energy loss. Chem Mater 2017;29:8369-76.

[59] McGehee MD, Bergstedt T, Zhang C, Saab AP, O'Regan MB, Bazan GC, et al. Narrow bandwidth luminescence from blends with energy transfer from semiconducting conjugated polymers to Europium complexes. Adv Mater 1999;11:1349-54.

[60] Kan B, Feng H, Wan X, Liu F, Ke X, Wang Y, et al. Small-molecule acceptor based on the heptacyclic benzodi(cyclopentadithiophene) unit for highly efficient nonfullerene organic solar cells. J Am Chem Soc 2017;139:4929-34.

[61] Li Z, Xu X, Zhang W, Meng X, Ma W, Yartsev A, et al. High performance all-polymer solar cells by synergistic effects of fine-tuned crystallinity and solvent annealing. J Am Chem Soc 2016;138:10935-44.

[62] Guo X, Facchetti A, Marks TJ. Imide- and amide-functionalized polymer semiconductors. Chem Rev 2014;114:8943-9021.

[63] Zhang K-N, Bi P-Q, Wen Z-C, Niu M-S, Chen Z-H, Wang T, et al. Unveiling the important role of non-fullerene acceptors crystallinity on optimizing nanomorphology and charge transfer in ternary organic solar cells. Org Electron 2018;62:643-52.

[64] Xiao Z, Jia X, Li D, Wang S, Geng X, Liu F, et al. 26 mA cm^{-2} J_{sc} from organic solar cells with a low-bandgap nonfullerene acceptor. Sci Bull 2017;62:1494-6.

NFAs with six-member-ring connection

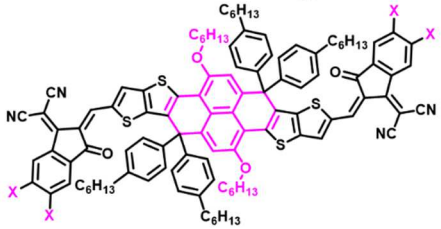

PTT-IC X = H
PTT-2FIC X = F